Mercapturate pathway metabolites of sotorasib, a covalent inhibitor of KRAS [G12C], are associated with renal toxicity in the Sprague Dawley rat

Jonathan A. Werner [a,*], Rhian Davies [a], Jan Wahlstrom [b], Upendra P. Dahal [b], Min Jiang [b], Jonathan Stauber [c], Benjamin David [c], William Siska [a], Barbara Thomas [d], Katsu Ishida [a], W. Griffith Humphreys [e], J. Russell Lipford [f], Thomas M. Monticello [a]

[a] Amgen Research, Translational Safety and Bioanalytical Sciences, Thousand Oaks, CA, USA
[b] Amgen Research, Pharmacokinetics and Drug Metabolism, South San Francisco, CA, USA
[c] Imabiotech Corp, Billerica, MA, USA
[d] Amgen Research Operations, Thousand Oaks, CA, USA
[e] Aranmore Pharma Consulting, Lawrenceville, NJ, USA
[f] Amgen Research, Oncology, Thousand Oaks, CA, USA

Visit us at AliriBio.com

ARTICLE INFO

ABSTRACT

Sotorasib is a first-in class KRAS [G12C] covalent inhibitor in clinical development for the treatment of tumors with the KRAS p.G12C mutation. In the nonclinical toxicology studies of sotorasib, the kidney was identified as a target organ of toxicity in the rat but not the dog. Renal toxicity was characterized by degeneration and necrosis of the proximal tubular epithelium localized to the outer stripe of the outer medulla (OSOM), which suggested that renal metabolism was involved. Here, we describe an in vivo mechanistic rat study designed to investigate the time course of the renal toxicity and sotorasib metabolites. Renal toxicity was dose- and time-dependent, restricted to the OSOM, and the morphologic features progressed from vacuolation and necrosis to regeneration of tubular epithelium. The renal toxicity correlated with increases in renal biomarkers of tubular injury. Using mass spectrometry and matrix-assisted laser desorption/ionization, a strong temporal and spatial association between renal toxicity and mercapturate pathway metabolites was observed. The rat is reported to be particularly susceptible to the formation of nephrotoxic metabolites via this pathway. Taken together, the data presented here and the literature support the hypothesis that sotorasib-related renal toxicity is mediated by a toxic metabolite derived from the mercapturate and β-lyase pathway. Our understanding of the etiology of the rat specific renal toxicity informs the translational risk assessment for patients.

1. Introduction

KRAS (Kirsten rat sarcoma viral oncogene homolog) (Kirsten and Mayer, 1967), the most frequently mutated oncogene in human cancer, encodes a small guanosine 5′triphosphate hydrolase (GTPase) signal transduction protein also called KRAS (Chang et al., 1982). Sotorasib is a first-in-class KRAS [G12C] covalent inhibitor that potently and selectively inhibits oncogenic signaling and growth and survival of tumors with the KRAS p.G12C mutation (Canon et al., 2019; Lanman et al., 2020). The KRAS p.G12C mutation has only been reported in tumor tissue and is not present in normal tissue (Barbacid, 1987; Karnoub and Weinberg, 2008;

AACR, 2017; Román et al., 2018). Sotorasib is highly selective for KRAS [G12C] versus wildtype KRAS with absence of any clinically relevant off-target binding (Canon et al., 2019). Therefore, no primary pharmacology-related on-target effects of sotorasib in normal "non-tumor bearing" animals or normal tissues in patients would be expected.

Recently, the U.S. Food and Drug Administration has granted Breakthrough Therapy designation for sotorasib in the treatment of patients with locally advanced or metastatic non-small cell lung cancer with the KRAS [G12C] mutation. As part of the nonclinical safety assessment, sotorasib was evaluated in 28-day and 3-month repeat-dose oral toxicology studies in the Sprague Dawley (SD) rat and the beagle dog

---

(unpublished data). In the rat toxicology studies, the kidney was identified as a target organ. No renal toxicity was observed in the dog. Renal toxicity in the rat was characterized by degeneration and necrosis of the proximal tubular epithelium localized to the outer stripe of the outer medulla (OSOM), a region of the nephron that is rich in metabolizing enzymes (Cooper and Hanigan, 2018; Lock and Antoine, 2018; Hanna and Anders, 2019). Compared to the 28-day rat study, the incidence and severity of the proximal tubular degeneration and necrosis increased in the 3-month study. There was no degeneration or necrosis in any other organ in the rat.

To investigate the pathogenesis and potential mechanism of the rat renal toxicity, a 7-day mechanistic rat study was conducted to evaluate the light microscopic time course of the renal changes, the metabolite profile (plasma, urine, and tissue), and potential correlations with both novel and routine kidney injury biomarkers. Our data support the hypothesis that sotorasib-related renal toxicity is mediated by a toxic metabolite derived from the mercapturate and β-lyase pathway.

2. Materials and methods

2.1. Test and control articles

Sotorasib was synthesized at Amgen, Inc., Thousand Oaks, CA (Canon et al., 2019; Lanman et al., 2020). The vehicle control article was 20% Captisol, pH 2.2 in reverse osmosis deionized water. Prior to dosing, sotorasib was suspended with the vehicle control at appropriate concentrations and dose formulation analysis was routinely performed to confirm expected test article concentration and homogeneity.

2.2. Animals

Similar to the previous 28-day and 3-month rat toxicology studies, the Sprague Dawley (Crl: CD[SD]) rat was used in the mechanistic study; only males were used because there was no sex-related difference in renal toxicity. All animals were housed at Association for Assessment and Accreditation of Laboratory Animal Care (AAALAC) international-accredited facilities. Rats were 10 weeks old at the initiation of dosing and were group-housed (up to 3 animals/cage) in solid bottom cages with bedding or individually housed as needed for study-related procedures. Animals had ad libitum access to water and pelleted feed, except for a 4-h food fast prior to blood collection at scheduled necropsy. All animals were maintained on a 12:12 h light:dark cycle in rooms with appropriate temperature (20 °C to 26 °C), humidity (30% to 70%) and ventilation (10 or more air changes per hour) controls. Prior to necropsy, animals were euthanized under deep anesthesia induced by isoflurane inhalation, followed by complete exsanguination.

2.3. Study design

The study was conducted at a contract research organization and approved by the local Institutional Animal Care and Use Committee. The design and execution of the study complied with all applicable sections of the Final Rules of the Animal Welfare Act regulations (Code of Federal Regulations, Title 9), the *Public Health Service Policy on Humane Care and Use of Laboratory Animals* from the Office of Laboratory Animal Welfare (OLAW, 2015), and the *Guide for the Care and Use of Laboratory Animals* from the National Research Council (NRC, 2011).

The study was designed to characterize the time-course of sotorasib-related renal tubular degeneration and necrosis over a 7-day period, and to investigative the association between the light microscopic renal tubular changes with blood and urine biomarkers of renal toxicity, as well as toxicokinetics (TK). In addition, sotorasib and its metabolites were analyzed in plasma, urine, kidney, and liver using mass spectrometry.

Dose levels corresponded to the low and high dose levels used in the 3-month rat toxicology study (Table 1). In Part 1 of the study, male rats

Table 1

Study design.

Test Material	Dose Level (mg/kg/day)	Number of Animals			
		Part 1[a]			Part 2[b]
Doses		1	3	7	1
Control	0	5	5	5	–
Sotorasib	60	5	5	5	–
Sotorasib	750	5	5	5	–
Control	0	–	–	–	9
Sotorasib	750	–	–	–	9

[a] Male Sprague Dawley rats in study part 1 received daily oral doses for 1, 3, or 7 days and were euthanized 24 h after the last dose.

[b] The animals in study part 2 received a single oral dose and 3 animals/group/time point were euthanized at 2, 4 or 8 h postdose.

(5 animals/group/timepoint) received daily oral gavage doses of sotorasib at 0, 60, or 750 mg/kg for 1, 3, or 7 days, and were euthanized 24 h after the last dose. In Part 2, rats (3 animals/group/timepoint) received a single oral gavage dose of sotorasib at 0 or 750 mg/kg and were euthanized at 2-, 4-, or 8-h post-dose.

In Part 1, toxicokinetic blood samples were collected pre-dose, and 0.5-, 1-, 2-, 8-, and 24-h after the last dose for each group. In Part 2, samples were collected at necropsy 2-, 4-, and 8-h post-dose. Plasma sotorasib concentrations were quantified using a validated LC-MS/MS method and noncompartmental analysis was performed using Phoenix WinNonlin (Pharsight Corporation, Mountain View, CA) to estimate TK parameters, including the maximum observed concentration (C_{max}) and the area under the concentration curve (AUC_{0-t}).

Study parameters evaluated both parts of the study included clinical observations, body weight, and light microscopic evaluation of the kidney. Additional parameters evaluated in Part 1 of the study included serum urea nitrogen (UN), creatinine, and electrolytes (sodium, potassium, and chloride); urine creatinine, glucose, and electrolytes (sodium and potassium); urine biomarkers of renal tubule injury (KIM-1, clusterin); kidney and liver weight; and light microscopic evaluation of the liver.

Prior to necropsy, urine was obtained via overnight collection on ice from urine collection cages and blood samples were collected from animals under isoflurane anesthesia. Blood samples for clinical chemistry were processed to serum and analyzed on a Cobas 6000 chemistry analyzer (Roche Diagnostics, Indianapolis, IN). Urine was analyzed on a Cobas 6000 chemistry analyzer (Roche Diagnostics) and urine KIM-1 and clusterin were measured on a Luminex Bio-Plex 200 (Bio-Rad Laboratories, Inc., Hercules, CA) using the Rat Kidney Toxicity Magnetic Bead Panel 1 Kit (MilliporeSigma, Burlington, MA). For urine glucose, KIM-1, and clusterin, both absolute concentrations and analyte/creatinine ratios were determined. For urine electrolytes, absolute concentration and fractional excretion, calculated as a percentage using the following formula: [(urine electrolyte concentration x serum creatinine concentration) / (serum electrolyte concentration x urine creatinine concentration)] x 100, were determined.

The kidney and liver were routinely processed to hematoxylin and eosin-stained slides for light microscopic evaluation. The histologic sections of kidney were evaluated subjectively based on a semi-quantitative 4-point severity scale (minimal, mild, moderate, and marked) in which the associated morphologic features of each score were distinct. To facilitate comparison of dose groups, the morphologic features of the sotorasib-related changes in the kidney were combined into the diagnostic term 'degeneration and necrosis.' Minimal and mild degeneration and necrosis was restricted to the OSOM and comprised of focal (<50% tubules affected) to diffuse (100% tubules affected) tubule epithelial vacuolation, respectively. Moderate degeneration and necrosis primarily involved the OSOM and included evidence of tubule regeneration (e.g. tubular basophilia and mitotic figures) mixed with occasional necrosis of tubule epithelium. Marked degeneration and necrosis was restricted to the OSOM and was characterized by complete

necrosis of the tubule epithelium variably associated with hyaline casts, and dystrophic mineralization. Hepatocellular hypertrophy was scored subjectively based on the amount of affected liver tissue and the relative increase in size of hepatocytes compared to concurrent controls.

Plasma, urine (Part 1 only), liver, and kidney tissue samples were collected for metabolite analysis by mass spectrometry. Samples of liver and kidney were taken at necropsy and snap frozen in liquid nitrogen. Frozen kidney samples were also collected for MALDI analysis.

2.4. Metabolite analysis

Metabolite characterization was conducted using liquid chromatography-high resolution mass spectrometry (LC-HRMS). Plasma samples were pooled across timepoints as previously described (Hamilton et al., 1981). A 240 μL sample of pooled plasma was quenched with 3 volumes of acetonitrile containing 0.1% formic acid. Urine samples were pooled from rats within the same dose levels and timepoint. A 240 μL sample of pooled urine was quenched with 3 volumes of acetonitrile containing 0.1% formic acid. Liver and kidney tissues were cut and weighed individually. Tissue samples were suspended in PBS at a ratio of 200 mg tissue to 1 mL of solvent followed by homogenization using a Qiagen Tissue Lyser II homogenizer (QIAGEN, Germantown, MD). Urine and tissue samples collected from all animals from the same dose at the same day were pooled by matrix type. Aliquots (250 μL) of the combined tissue sample were extracted with 3 volumes (750 μL) of acetonitrile (containing 0.1% formic acid). The quenched sample mixtures were vigorously mixed for 15 min, followed by centrifugation at 3220 xg for 15 min. A portion of supernatant (200 μL) was used for analysis using LC-HRMS injection. Another portion of supernatant (600 to 800 μL) was evaporated to dryness under nitrogen at 37 °C. The dried samples were reconstituted in 200 μL of 50% water, 50% methanol solution containing 0.1% formic acid and analyzed by LC-HRMS. Agilent 1290 (Agilent Technologies, Santa Clara, CA) and Thermo CTC HTS PAL (Thermo Fisher Scientific, Waltham, MA) were used as HPLC and autosampler. Mobile phase A and B were water and acetonitrile, both containing 0.1% of formic acid. A 60 min LC gradient was used with a 250 mm Waters Atlantis T3 column (Waters Corporation, Milford, MA) with a particle size of 5 μM. Orbitrap Q Exactive HRMS (Thermo Fisher Scientific) was used for MS data collection. Structural assignments for excreted metabolites were determined via mass spectral analysis. The percent of drug related material (% DRM) for sotorasib and individual sotorasib metabolites was estimated by dividing each mass spectrometry peak by the sum of all peak areas.

2.5. Matrix-assisted laser desorption/ionization analysis (MALDI) of sotorasib metabolites in the kidney

Sectioning of snap-frozen kidneys (N = 3/group/timepoint from Part 1 and 2 of the study) was performed using a cryostat (Leica, Buffalo Grove, IL) at −20 °C. For each kidney, 10 μm sections were collected on indium tin oxide (ITO) conductive glass slides (Delta Technologies, Loveland, CO) for MALDI mass spectrometry imaging (MSI) and on Superfrost slides (Fischer Scientific) for routine hematoxylin and eosin staining. Sections mounted on ITO slides were placed in a desiccator for 20 mins. Then, the slides were sprayed with a solution of 2,5-dihydroxbenzoic acid (Sigma-Aldrich) at 40 mg/mL in 1:1 methanol:1% trifluoroacetic acid v/v using an automatic TM Sprayer (HTX Imaging, Chapel Hill, NC). The settings of the TM Sprayer were 90 μL/min flow rate, 75 °C for nozzle temperature, and 12 layers.

MALDI MSI analysis was performed for the detection of sotorasib and sotorasib metabolites using a Solarix 7 T MALDI-FTICR (Bruker Daltonics, Billerica, MA) equipped with a Smartbeam II laser at a repetition rate at 2000 Hz. For the detection of the sotorasib, mass spectra were acquired in positive mode with a Continuous Accumulation of Selected Ions (CASI) mode of acquisition within m/z 556 to 576 Da range and a spatial resolution of 100 μm. For the detection of its metabolites, mass spectra were acquired in positive full scan mode of acquisition within m/z 0 to 1000 Da range at a spatial resolution of 100 μm. The mass spectrum obtained for each position of the images corresponded to the averaged mass spectra of 300 consecutive laser shots on the same location. Bruker software packages including FlexControl 2.2.0 and FlexImaging 5.0 were used for recording the data and the previsualization of the data.

Multimaging™ 1.2.5.9 (ImaBiotech, Boston, MA) was used to create the molecular distributions, determine relative quantitation, conduct statistical analysis, and identify metabolites. For each molecular image, the intensity scale was adjusted to eliminate background by increasing the lower threshold and to maximize information for visualization by
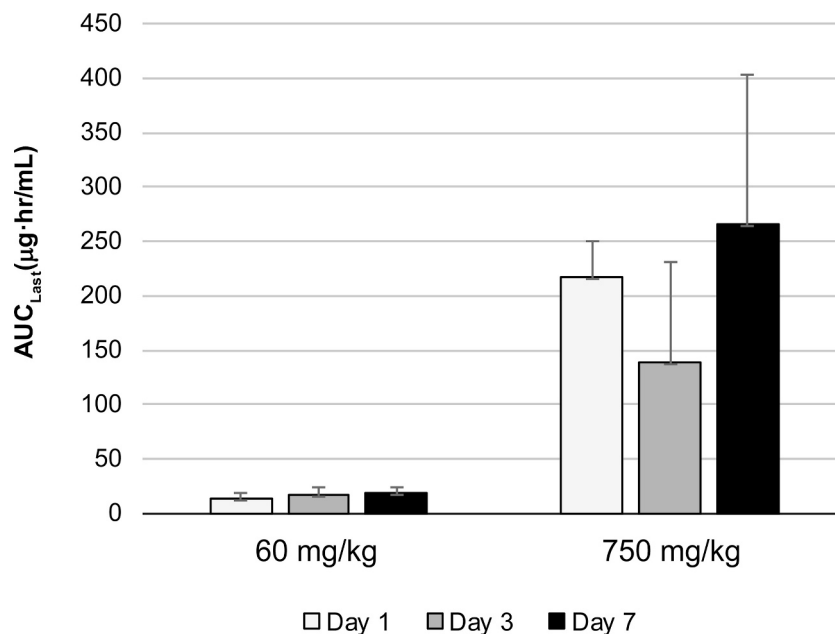

Fig. 1. Sotorasib systemic exposure. Group mean sotorasib exposure, as measured by area under the concentration-time curve from time zero to the last quantifiable concentration up to 24 h (AUC_{last}), in the 7-day rat mechanistic study. Error bars = standard deviation.

decreasing the upper threshold. The convolution was conducted on the original images using a normalized uniform kernel which averages the values around a position. The kernel size was manually optimized for the analysis minimizing the background noise and the relative quantifications of the targeted molecules were extracted from the region of interest.

2.6. Statistical analysis

Statistical analysis of body weight, organ weight, and clinical pathology data included routine descriptive and inferential statistical analysis. Statistical analyses were performed in GraphPad Prism 8.4.3 (GraphPad Software, San Diego, CA). The Brown-Forsythe test was used to assess the homogeneity of group variances. The groups were compared using an overall one-way ANOVA F-test in case of homogeneity or the ANOVA Welch test in case of heterogeneity with Dunnett's or Dunn's correction, respectively, to control for Type I error. The Kruskal-Wallis test was used in case of non-normality with Dunn's correction. One-sample Wilcoxon test was used to test against groups with identical entries. For values that were below the lower limit of

detection of the assay, the value was assigned as the lower limit for statistical tests. Statistical significance was defined as $p < 0.05$. For MALDI-MSI data, a *t*-test was conducted using Multimaging™ 1.2.5.9 comparing signal intensity in the kidney at 0 and 750 mg/kg. Three replicate samples at 2-, 4- and 8-h post-dose in study Part 2 were combined for each dose level to assess statistical significance of *m/z* values. Statistical tests were not conducted for MALDI data at 60 mg/kg because no signal was identified. Statistical analysis of semi-quantitative histology data and LC-HRMS metabolite data was not conducted.

3. Results

3.1. Sotorasib-related renal toxicity in the rat was time- and dose-dependent

The 7-day mechanistic study in the rat was conducted to investigate the relationship of sotorasib metabolites to renal toxicity (toxicology data provided in Supplementary Table 1). There were no clinical observations or unscheduled deaths at 60 mg/kg. In contrast, signs of poor clinical condition (e.g. hunched posture, decreased activity) were
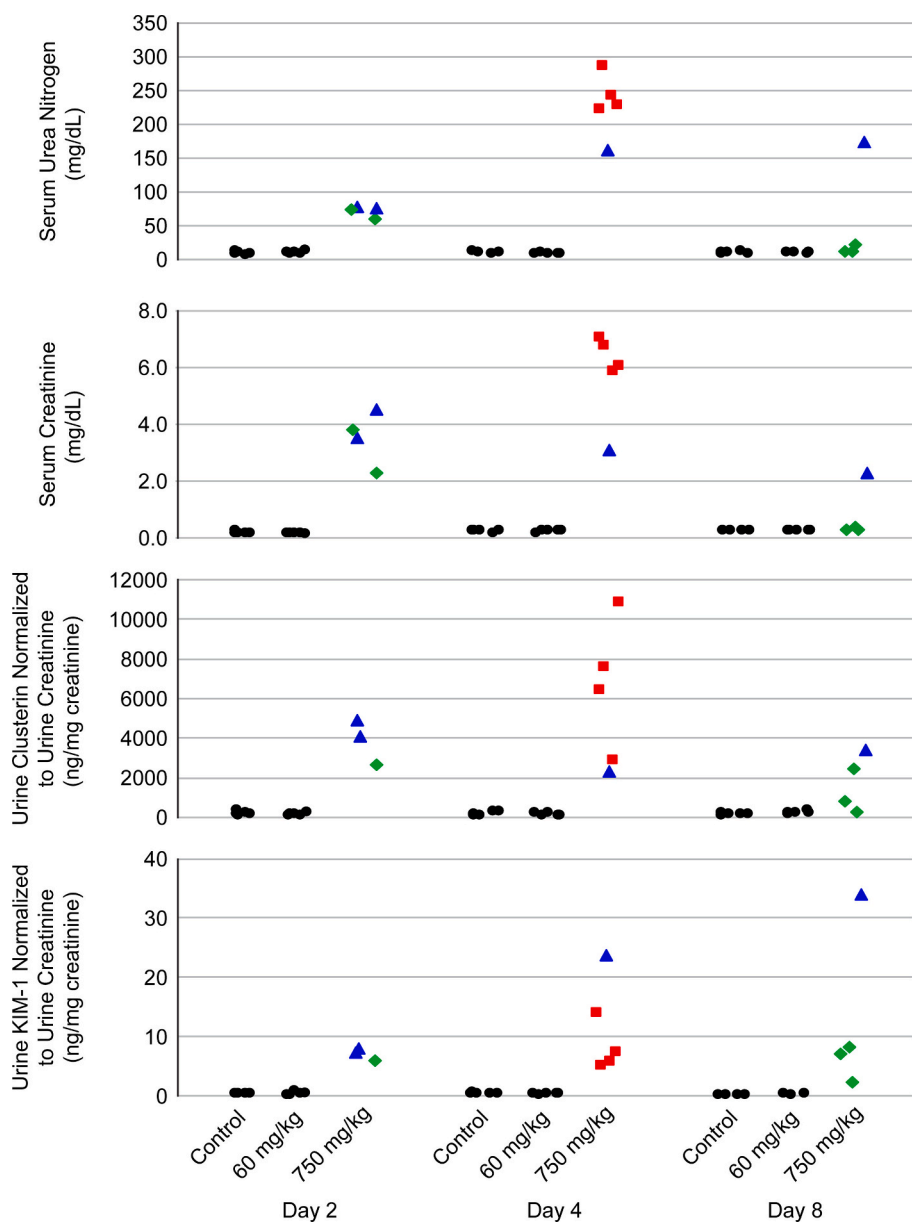
Fig. 2. Biomarkers associated with sotorasib-related renal toxicity. Data for individual rats are shown for serum urea nitrogen, serum creatinine, urine clusterin (normalized to urine creatinine) and urine kidney injury molecule-1 (KIM-1; normalized to urine creatinine), separated by dose level at each time point assessed (study days 2, 4, and 8). The severity of light microscopic change of tubular degeneration and necrosis in the kidney for each animal is represented by shape and color of the marker: within normal limits (black circle), mild (green diamond), moderate (blue triangle), marked (red square). There were no changes in these endpoints at 60 mg/kg. At 750 mg/kg, there were increases in all four endpoints, generally reaching the largest magnitude by study day 4 (after 3 days of dosing). On day 2 at 750 mg/kg, no blood was obtained from 1 of 5 animals due to technically difficulties and there was insufficient urine collected from 2 of 5 animals. (For interpretation of the references to color in this figure legend, the reader is referred to the web version of this article.)
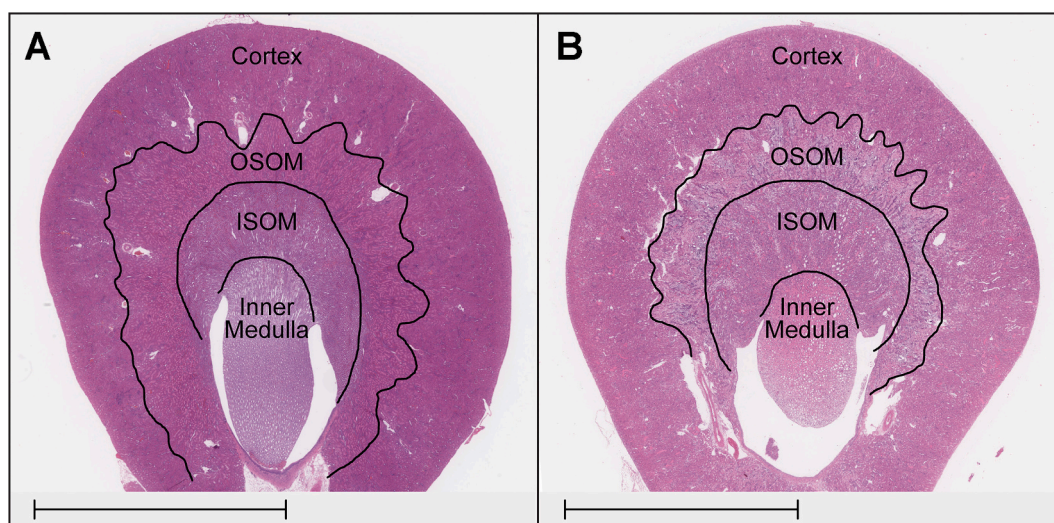
Fig. 3. Sotorasib-related tubular epithelial degeneration and necrosis was primarily observed in the outer stripe of the outer medulla. Representative photomicrographs of the kidney from a control animal (A), and an animal 24 h after administration of 750 mg/kg of sotorasib (B). Dotted lines show the approximate boundaries between the cortex, the outer stripe of the outer medulla (OSOM), the inner stripe of the outer medulla (ISOM), and the inner medulla. The tubules in the OSOM at 750 mg/kg are pale as a result of epithelial cell necrosis. Scale bar = 5 mm.

observed at 750 mg/kg from day 3 until terminal necropsy and resulted in an early euthanasia of one animal. After 7 daily doses, there was a statistically significant mean body weight loss of 19% in animals at 750 mg/kg compared to concurrent controls.

Sotorasib systemic exposure was maintained for the duration of the study, AUC_{0-t} increased in a dose-proportional manner, and accumulation from day 1 to day 7 was <2-fold (Fig. 1). Exposure at 750 mg/kg over the 8-h time period of study Part 2 was comparable to the exposure at this dose level in study Part 1.

There were no clinical or anatomic pathology changes at 60 mg/kg. At 750 mg/kg there was an increase in kidney weight (44% to 86%), and bilateral pale discoloration of the kidneys. Clinical pathology parameter changes at 750 mg/kg included an increase in serum UN and creatinine, and an increase in urine KIM-1 and clusterin (absolute and normalized to creatinine) (Fig. 2). Additional changes at 750 mg/kg included an increase in urine glucose (normalized to creatinine and absolute) and fractional excretion of sodium and potassium, and a decrease in serum chloride and increase in serum potassium. Sotorasib-related changes in organs weights and clinical pathology parameters were generally statistically significant.

By light microscopy, acute degeneration and necrosis of epithelial cells, primarily restricted to the proximal tubules in the OSOM, was observed at 750 mg/kg only (Fig. 3). The histopathologic changes in the kidneys correlated with the increased kidney weight and the macroscopic observations. The incidence and severity of the renal tubular

Table 2
Incidence and severity of sotorasib-related renal toxicity at 750 mg/kg.

Timepoint (hour or day)	Hour			Day		
	2	4	8	2	4	8
Number of animals examined	3	3	3	5	5	4[a]
Degeneration/necrosis; tubule						
Minimal	1	–	–	–	–	–
Mild	–	3	3	–	–	–
Moderate	–	–	–	–	–	3
Marked	–	–	–	5	5	1

- = no sotorasib-related findings.

[a] One animal with marked degeneration/necrosis was euthanized early on study day 3 due to poor clinical condition attributed to renal toxicity. This animal is not included in this table.

changes were dose- and time-dependent (Table 2). The morphologic features observed at 2 to 8 h after a single dose consisted of minimal (focal) to mild (diffuse) renal tubular epithelial vacuolation located in the OSOM (Fig. 4). At 24 h after a single dose, there was marked necrosis of proximal tubular epithelium involving the entire OSOM. With repeated dosing, marked necrosis was accompanied by tubular lumen hyaline casts, dystrophic mineralization, and evidence of progressive epithelial regeneration (e.g. basophilic tubular epithelium, mitotic figures). At the end of the study (day 8), there was evidence of tubular regeneration (e.g., tubular basophilia, mitotic figures, and nuclear crowding) mixed with occasional acute degeneration and necrosis of individual proximal tubular cells (moderate). In addition, one animal at day 8 had a large band of dystrophic mineralization in the OSOM. At all timepoints, the tubular epithelial cells lining the thick ascending limb of the loop of Henle and the collecting ducts, which also pass through the OSOM, were nonremarkable, indicating that the tubular epithelial insult was restricted to the proximal tubules.

On day 4, there was minimal diffuse hepatocellular hypertrophy (with mitotic figures) in the liver at 750 mg/kg, which correlated with a statistically significant increase in absolute and relative (to body weight) liver weight (~46%). The increased liver weight associated with hepatocellular hypertrophy was interpreted as an adaptive response of hepatic P450 enzyme induction (Maronpot et al., 2010).

There was a clear association between renal toxicity and statistically significant increases in serum UN and creatinine, as well as increases in renal injury biomarkers KIM-1 and clusterin in urine. Increases in these endpoints were observed at 750 mg/kg, as early as 24 h after a single dose, and were generally increased to a greater extent after 3 days of dosing. This pattern of increase was consistent with the time course of degeneration and necrosis of renal tubules.

3.2. Mercapturate pathway metabolites of sotorasib constituted a higher proportion of drug-related material in the kidney and urine at the toxic dose level

Sotorasib-related metabolites were identified in samples of plasma, urine, kidney and liver and proposed structures were based on the m/z and mass shift from parent, as well as general knowledge of metabolism (Supplementary Table 2). Using these structures, a generalized metabolic scheme for sotorasib was constructed (Fig. 5). Sotorasib metabolism follows one of several initial metabolic transformations
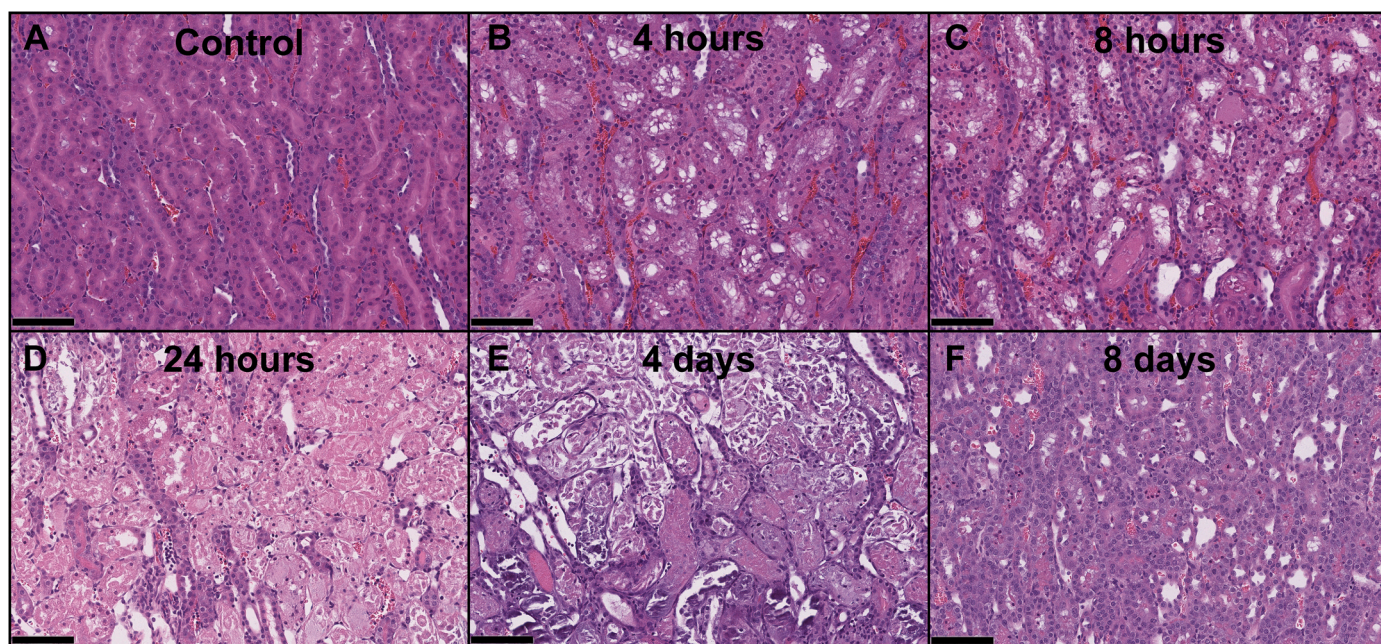
Fig. 4. Time-course of sotorasib-related renal toxicity at 750 mg/kg. Representative photomicrographs of tubules in the outer stripe of the outer medulla (OSOM) from a control animal (A), and animals administered 750 mg/kg of sotorasib and euthanized at different timepoints. At 2, 4 and 8 h, there was focal (minimal) to diffuse (mild; B and C) vacuolation of proximal tubular epithelium with variable hyaline and granular cast formation in tubule lumens. At 24 h (D), the renal toxicity was characterized by acute necrosis of proximal tubules involving the entire OSOM. Distal tubules were lined by intact epithelium. At 4 days (E), the proximal tubules were filled with necrotic cellular debris that was frequently mineralized and the tubular basement membranes were often lined by flattened regenerative epithelium. At 8 days (F), there was reduced mineralization and evidence of progressive repair of the epithelial damage (e.g., tubular basophilia, mitotic figures, and nuclear crowding) mixed with occasional acute degeneration and necrosis of individual proximal tubular cells. Scale bar = 100 μm.

including: dealkylation and cleavage (M24), direct reduction of the acrolein moiety (M21), oxidation (M18), lysine conjugation (M62), or glutathione conjugation (M12). Following the initial transformation, some metabolites undergo further biotransformation, including metabolism of M12 by enzymes of the mercapturate pathway to yield cysteinylglycine conjugate M30, cysteine conjugate M10, and acetylcysteine conjugate M20.

The metabolite profiles in the samples were compared across dose level and time to explore associations with renal toxicity. This comparison demonstrated a dose- and time-related association between renal toxicity and mercapturate pathway metabolites of glutathione conjugate M12. In the kidney at 2- to 8-h after a single nephrotoxic dose, mercapturate pathway metabolites (M10, M20, M61, and M63) comprised >83% DRM; parent sotorasib was ~10% DRM or less and all other metabolites were individually <1.0% DRM (Table 3). At 24 h, mercapturate pathway metabolites constituted a higher proportion of total metabolites at the nephrotoxic dose of 750 mg/kg compared to the non-toxic dose of 60 mg/kg. The relative proportion of mercapturate pathway metabolites and sotorasib decreased over time with repeated dosing, associated with an increasing proportion of lysine conjugate M62. By day 8, there were reduced proportions mercapturate pathway metabolites, and evidence of tubular regeneration. At the non-nephrotoxic dose level, the mercapturate pathway metabolites comprised a smaller proportion of the % DRM, largely due to the presence of M62 and smaller contributions from other unrelated biotransformations. Taken together, M62 was not considered to be a contributing factor to nephrotoxicity. In the urine collected after 1, 3, or 7 daily doses, there was a similar increased proportion of mercapturate pathway metabolites at the nephrotoxic dose level (Table 4). Sotorasib metabolites associated with the mercapturate pathway metabolites comprised the majority of DRM, while other metabolites generally contributed <5% DRM. Taken together, the metabolite profile in the kidney and urine demonstrate a strong association between mercapturate pathway metabolites and renal toxicity.

In plasma, the most prominent circulating metabolites (>10% DRM) were M10 (cysteine conjugate) and M24 (des(methylpiperazinylpropenone)-sotorasib dione), while M12 (glutathione conjugate) was a minor circulating metabolite (Supplementary Table 3). There was no apparent difference in relative metabolite proportions in plasma between 60 and 750 mg/kg. In the liver, most metabolites in the proposed scheme were identified; however, total mercapturate pathway metabolites, including M10, were in higher proportions at 750 mg/kg compared to 60 mg/kg (Supplementary Table 4). The metabolite profile in the liver was not associated with liver toxicity.

3.3. Mercapturic pathway metabolites are temporally and spatially associated with renal toxicity by MALDI analysis

MALDI analysis of the kidney identified a strong temporal and spatial association between OSOM restricted renal injury and the presence of downstream metabolites of glutathione conjugate M12. At 60 mg/kg, there were no MALDI signals for sotorasib or sotorasib metabolites at any timepoint evaluated, nor was there any light microscopic evidence of renal tubular injury. At 750 mg/kg, sotorasib and mercapturate pathway metabolites M10 and M20 were identified in the kidneys (Fig. 6). At 2-, 4-, and 8-h after a single dose, sotorasib was observed throughout the kidney. In contrast, M10 and M20 were restricted to the OSOM (2 and 4 h only). For sotorasib, M10, and M20, the intensity signal was statistically significantly increased compared to concurrent controls (sotorasib p value = 0.0002; M10 p value = 0.0146; M20 p value = 0.0020). Twenty-four hours after a 1, 3, or 7 daily doses, sotorasib and M10 were still observed, but the patterns were patchy and not restricted to any particular part of the kidney. This pattern was attributed to widespread necrosis of proximal tubular epithelium in the OSOM and loss of function of these cells.
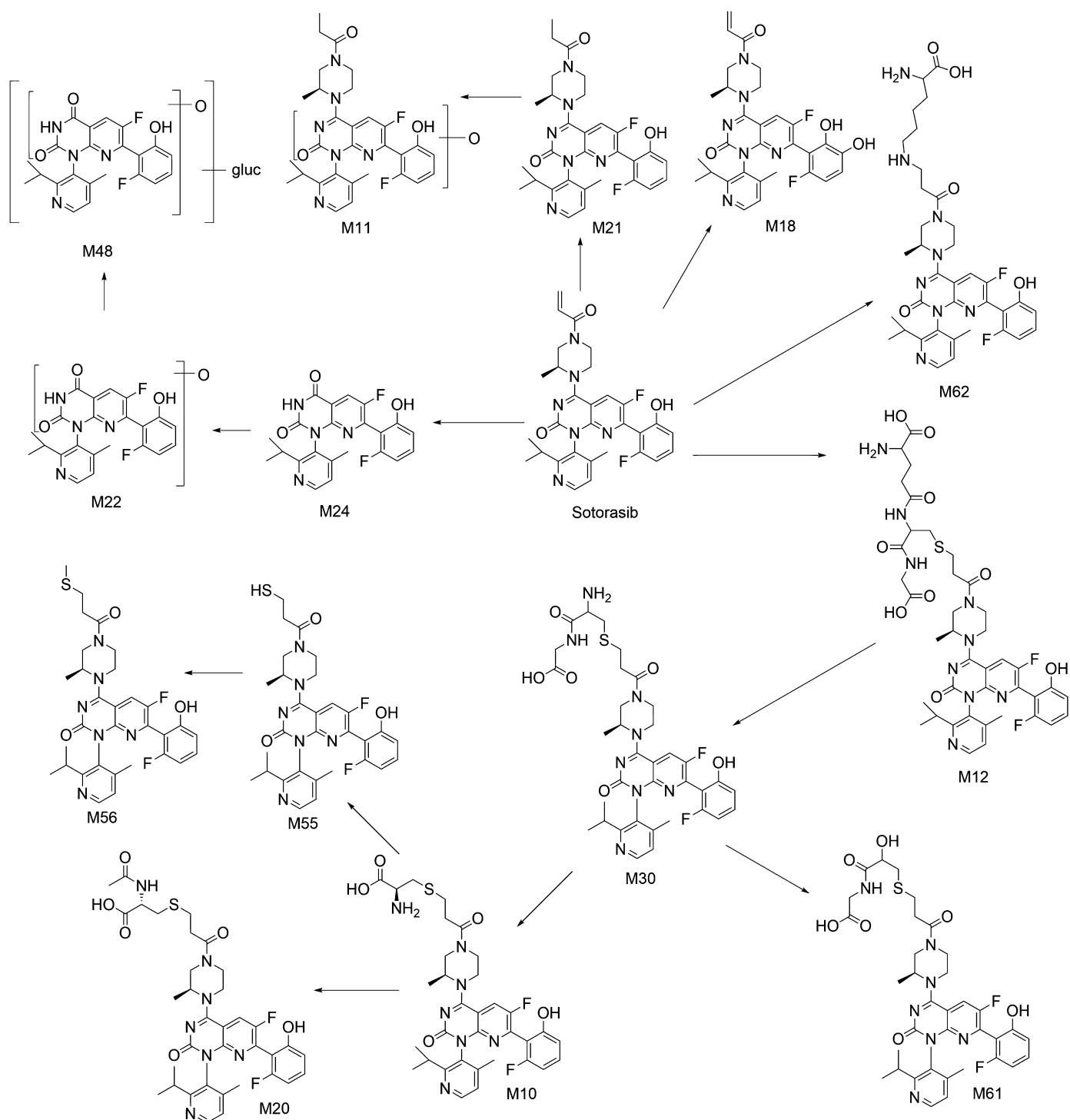
Fig. 5. Proposed metabolic scheme for sotorasib. Sotorasib metabolism follows one of several initial metabolic transformation including: dealkylation and cleavage (M24), direct reduction of the acrolein moiety (M21), oxidation (M18), lysine conjugation (M62), or glutathione conjugation (M12). Subsequent amide hydrolysis of the glutamate of M12 produces the cysteinylglycine conjugate M30. Sequential hydrolysis of M30 yields the cysteine conjugate M10 and *N*-acetylation of M10 results in mercapturic acid M20. Alternatively, cysteine cleavage of M10 yields M55 (not identified) and methylation of M55 results in the methylthio derivative M56. Oxidative deamination of M30 can also yield the hydroxy-cysteinylglycine conjugate M61. Lysine conjugation at the acrolein moiety produces lysine conjugate M62. Dealkylation and cleavage of sotorasib at the piperazine ring produces des(methylpiperazinylpropenone)-sotorasib dione M24. Secondary oxidation of M24 yields des (methylpiperazinylpropenone)-oxy-sotorasib dione metabolite M22. Glucuronidation of M22 produces the corresponding M22-glucuronide M48. Direct reduction of sotorasib on the acrolein moiety produces dihydro-sotorasib metabolite M21 while oxidation of sotorasib on the fluorophenol ring yields catechol metabolite M18. Oxidation of M21 yields M11.

Table 3
Percent drug-related material in the kidney.

Dose	60 mg/kg			750 mg/kg					
Timepoint	Day 2	Day 4	Day 8	2 Hr	4 Hr	8 Hr	Day 2	Day 4	Day 8
Sotorasib	3.3	2.1	2.7	10.3	5.1	1.4	<1.0	<1.0	<1.0
M10*	35.7	20.2	9.8	8.1	9.8	7.7	81.3	78.7	50.6
M20*	2.0	<1.0	<1.0	37.2	24.0	14.8	2.9	2.8	1.3
M61*	2.8	<1.0	<1.0	36.1	49.0	61.8	7.2	4.2	2.1
M63*	1.0	<1.0	<1.0	2.3	3.6	3.0	1.7	1.7	1.27
M56*	4.8	1.5	1.9	<1.0	<1.0	<1.0	<1.0	<1.0	<1.0
M62	28.4	65.5	77.4	<1.0	<1.0	<1.0	1.9	7.9	39.7
M22	6.1	2.1	<1.0	<1.0	<1.0	<1.0	<1.0	<1.0	<1.0
M21	7.3	1.5	4.8	<1.0	<1.0	<1.0	<1.0	<1.0	<1.0
M24	3.0	1.8	2.4	<1.0	<1.0	<1.0	<1.0	<1.0	<1.0
% MPM	46.3	21.7	11.7	83.7	86.4	87.3	93.1	87.4	55.3

* Metabolite associated with the mercapturate pathway; %MPM = percent mercapturate pathway metabolites.

Table 4
Percent drug-related material in the urine.

Dose	60 mg/kg			750 mg/kg		
Timepoint	Day 2	Day 4	Day 8	Day 2	Day 4	Day 8
Sotorasib	36.3	29.2	28.1	23.8	32.2	12.3
M10*	5.4	1.7	1.2	21.6	40.7	44.7
M20*	13.1	12.1	16.6	9.6	5.3	10.1
M61*	6.0	7.0	7.4	9.5	<1.0	2.9
M30*	<1.0	6.4	6.7	12.0	4.1	12.2
M31*	<1.0	1.9	1.1	2.0	<1.0	<1.0
M56*	<1.0	1.3	1.0	<1.0	<1.0	<1.0
M62	<1.0	7.0	11.6	<1.0	<1.0	<1.0
M37	<1.0	<1.0	1.3	1.3	1.2	1.9
M3	<1.0	<1.0	<1.0	1.5	1.0	1.3
M6	<1.0	<1.0	1.1	<1.0	<1.0	<1.0
M9	2.5	2.6	<1.0	<1.0	<1.0	<1.0
M4	<1.0	1.6	1.2	5.7	2.2	2.8
M48	1.6	2.8	3.2	3.2	1.8	4.3
M13	<1.0	<1.0	<1.0	1.9	1.8	2.0
M16	1.3	<1.0	<1.0	<1.0	<1.0	<1.0
M18	7.4	4.3	1.7	1.1	1.0	<1.0
M52	3.1	2.6	1.2	<1.0	<1.0	<1.0
M22	2.9	1.8	2.9	<1.0	1.4	<1.0
M21	11.5	8.3	6.6	<1.0	<1.0	<1.0
M24	1.4	1.2	1.3	<1.0	<1.0	<1.0
% MPM	24.5	30.4	34.0	54.7	50.1	69.9

* Metabolite associated with the mercapturate pathway; %MPM = percent mercapturate pathway metabolites.

4. Discussion

Sotorasib, a highly selective small molecule inhibitor that covalently binds to KRAS[G12C], was not associated with primary pharmacology-related on-target effects in normal "non-tumor-bearing" animals in toxicology studies. However, the kidney was identified as a sotorasib-related target organ of toxicity in the rat. The morphologic features of the kidney toxicity, including the restriction to the OSOM, suggested that renal metabolism was involved. Moreover, this toxicity was not observed in the dog, indicting a species-specific mechanism. Results of our time-course mechanistic investigation, including light microscopic characterization and detailed metabolite analyses, support the hypothesis that sotorasib-related renal toxicity in the rat is mediated by a nephrotoxic metabolite derived from the mercapturate and β-lyase pathway. The rat has been reported to be particularly susceptible to nephrotoxicity induced by β-lyase-mediated bioactivation, leading to the formation of potentially reactive free thiols and further downstream electrophilic metabolites (Cooper and Hanigan, 2018; Baillie, 2020; Rood et al., 2020).

Sotorasib-related renal toxicity in the rat was characterized by tubular epithelial cell degeneration and necrosis primarily restricted to the proximal tubules in the OSOM. This portion of the nephron, also known as the S3 segment or pars recta, is rich in metabolizing enzyme (Cooper and Hanigan, 2018). The thick ascending limb of the loop of Henle and the collecting ducts, which also pass through the OSOM, were not affected. Taken together, the histopathologic features of this toxicity indicate that a very specific region of the nephron was affected and that metabolism of sotorasib likely contributes, as observed with other nephrotoxicants in the rat such as halogenated alkenes and cisplatin (Cooper and Hanigan, 2018; Lock and Antoine, 2018).

Based on the mass spectrometry data in this study, the proposed metabolic scheme of sotorasib includes metabolic transformations mediated by mercapturate pathway enzymes; only these metabolites were associated with renal toxicity. Mercapturate pathway transformations of sotorasib begin with the binding of glutathione to the acrylamide warhead of sotorasib to form glutathione conjugate M12, followed by additional biotransformation to form cysteinylglycine conjugate M30, cysteine conjugate M10, and the mercapturic acid M20. These metabolites comprised a higher proportion of drug-related material in the rat kidney and urine at the nephrotoxic dose level (750 mg/kg) compared to the non-toxic dose level (60 mg/kg). Although absolute levels were not determined, it is reasonable to assume that mercapturate pathway metabolites were much higher at the nephrotoxic dose level compared to the non-nephrotoxic dose level. The increase in renal mercapturate pathway metabolites was evident as early as 2 h after a single dose and remained high for the study duration, correlating with histopathological features of progressive renal tubular epithelial toxicity (e.g. vacuolar degeneration progressing to cell necrosis). Mercapturate metabolites were also observed in the liver, but there was no evidence of hepatocellular injury, indicating that additional factors unique to the kidney are required for toxicity. However, formation of M12, M10, and M20 in the liver at the nephrotoxic dose level may have contributed to greater transportation of these metabolites to the kidney. MALDI analysis also demonstrated a temporal and spatial association between renal tubular injury of the OSOM and mercapturate pathway metabolites. Mercapturate pathway metabolites M10 and M20 were restricted to the OSOM in the rat kidney as early as 2-h postdose, whereas the parent sotorasib or other major metabolites were not. Metabolites unrelated to the mercapturate pathway, such as M24, M21, M18, or M62, were either absent or at low levels in the kidney and urine at the nephrotoxic dose level, indicating that they are not associated with renal toxicity and do not likely play a role. Although the parent molecule, sotorasib, does not appear to be directly toxic, it may have been converted to a reactive metabolite via the mercapturate pathway within the kidney, contributing to the renal toxicity. Taken together, the data demonstrate a strong association with mercapturate pathway metabolites, and no association with the parent molecule or other metabolites.

Although the putative rat-specific toxic metabolite was not identified in this study, the literature on nephrotoxicants provides possible mechanisms and contributing factors. A common metabolic pathway associated with renal toxicity in the rat includes transformations
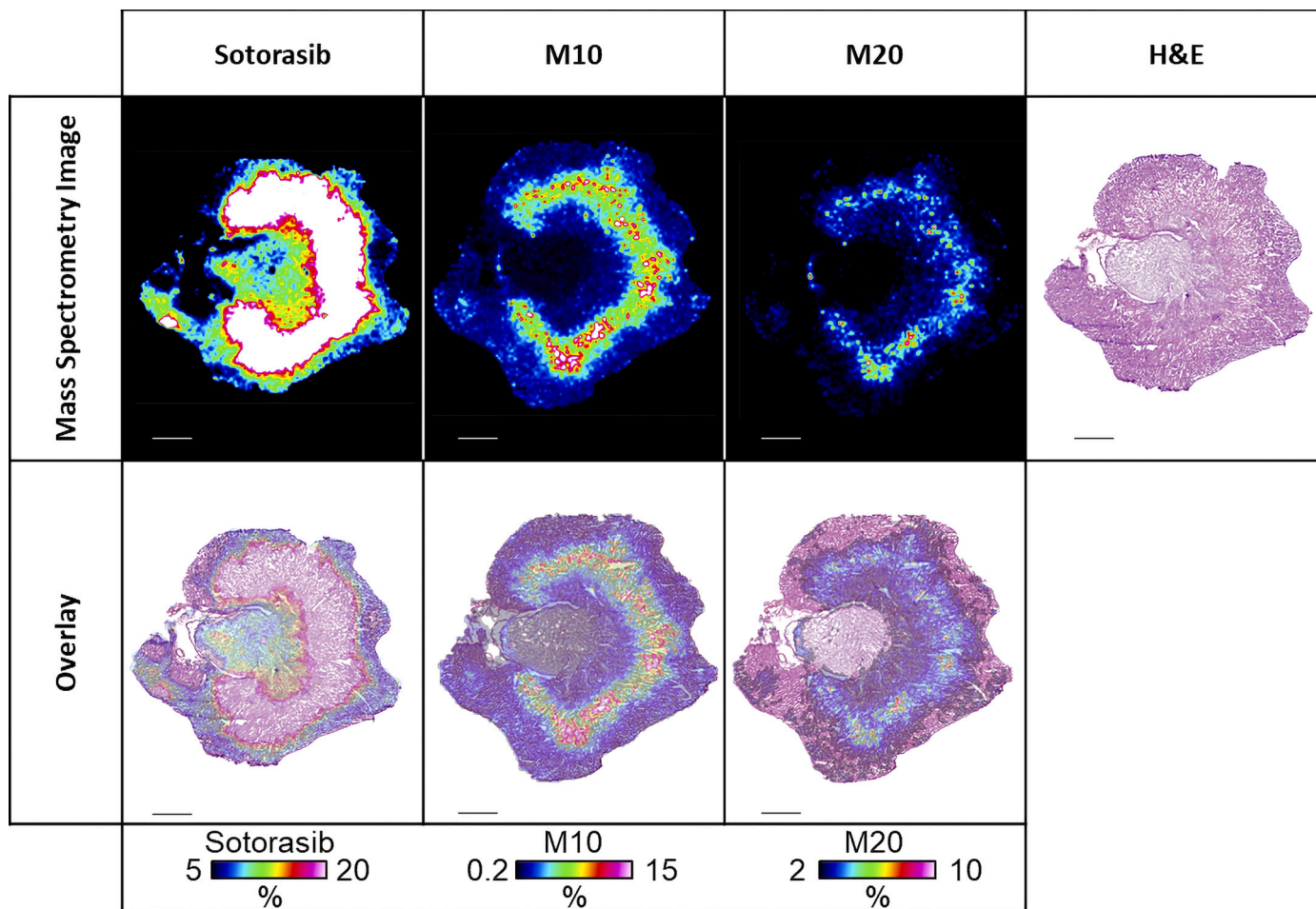
Fig. 6. Molecular distribution of sotorasib and mercapturate pathway metabolites M10 and M20. Representative images of MALDI analysis of rat kidney 4 h after a 750 mg/kg oral dose of sotorasib. The color intensity represented in the color scale is based on the mass spectrometry response for each analyte with the percentage correlating to the relative amount. The scales are adjusted at the low end (black) to remove background noise and at the high end (white) to optimize visualization of the distribution of the analyte. Overlay images are combined mass spectrometry image and hematoxylin and eosin (H&E) image. Scale bar = 1.6 mm.

involving the mercapturate pathway followed by generation of a reactive metabolite by β-lyases (Cooper and Hanigan, 2018). In general, formation of reactive metabolites via the mercapturate and β-lyase pathway begins with glutathione conjugation in the circulation and tissues (Cooper and Hanigan, 2018). Formation of glutathione S-conjugates can occur spontaneously (Michael addition), but the reaction is accelerated by glutathione S-transferases, a family of enzymes that catalyzes the reaction of the cysteinyl anion of glutathione with an electrophile. These reactions generally occur in the liver but can also occur in the S3 segment of the proximal tubule (Lock and Antoine, 2018). As the glutathione S-conjugates pass through the kidney, they are sequentially cleaved by gamma glutamyl transpeptidase to cysteinylglycine S-conjugates and aminodipeptidase to cysteine S-conjugates. In the rat, both gamma glutamyl transpeptidase and aminodipeptidases are localized in high concentration on the brush border membrane of the proximal tubular epithelium (Cooper and Hanigan, 2018; Lock and Antoine, 2018). As a final step, cysteine S-conjugates are reabsorbed by tubular epithelium and *N*-acetylated to the corresponding *N*-acetyl-L-cysteine S-conjugate (aka the mercapturate).

The mercapturate is generally more water soluble than the parent compound and more readily excreted into urine, as a detoxification step (Cooper and Hanigan, 2018). However, as parent and glutathione conjugate exposures increase, greater levels of intracellular cysteine S-conjugates would be expected to saturate mercapturate pathway detoxification. The excess cysteine S-conjugates would then be available for metabolism by renal β-lyase in the proximal tubule epithelium to

form a sulfur-containing thiol and additional downstream metabolites, which could be chemically reactive (Cooper and Hanigan, 2018; Lock and Antoine, 2018; Baillie, 2020). The reactive metabolites could covalently bind to cellular macromolecules leading to disruption of cellular processes, and cell death. Alternatively, less reactive thiols may be inactivated by thiol methyltransferases or glucuronosyltransferases, and subsequently eliminated (Cooper and Hanigan, 2018).

There are many toxicants that are dependent on the mercapturate and β-lyase pathway for formation and subsequent toxicity in the kidney (Horvath et al., 1992; Townsend and Hanigan, 2002; Tsuchida, 2002; Zhang and Hanigan, 2003; Miller et al., 2010; Testa and Clement, 2015; Barnett and Cummings, 2018; Cooper and Hanigan, 2018; Lock and Antoine, 2018; Perazella, 2018). One relevant example is ibrutinib, a small molecule anticancer covalent inhibitor with the same acrylamide warhead as sotorasib, for which nephrotoxicity was recently proposed to be dependent on the intracellular accumulation of the cysteine metabolite followed by formation of reactive electrophilic metabolites via the β-lyase pathway (Baillie, 2020; Rood et al., 2020).

Based on this general scheme for the generation of nephrotoxic metabolites, our proposed mechanism by which the mercapturate and renal β-lyase pathway convert sotorasib into a nephrotoxic metabolite is depicted in Fig. 7. In this scheme, nephrotoxic dose levels of sotorasib would contribute to the greater disposition of the cysteine-conjugate M10 in renal tissue and β-lyase-mediated bioactivation. The putative reactive sotorasib metabolite was not identified in this study. In other sotorasib metabolite studies in the rat, the thiol M55 was observed in the
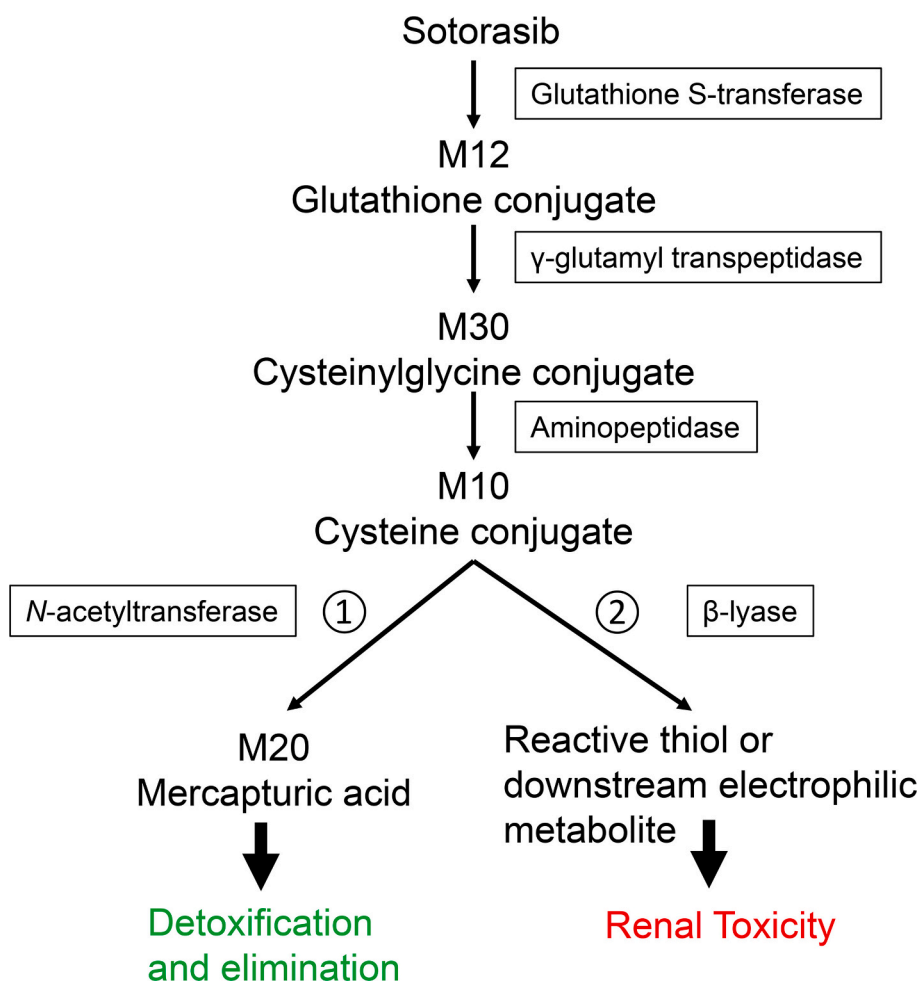
Fig. 7. Proposed metabolic scheme for sotorasib-related renal toxicity in the rat. Sotorasib is metabolized to the cysteine conjugate M10 via the mercapturate pathway or direct conjugation to cysteine. Nontoxic levels of M10 are further metabolized in renal tubular epithelial cells to the mercapturate (1) and eliminated in urine. At toxic dose levels, excess M10 in the renal tubular epithelial cells would be available for metabolism by renal β-lyase in the proximal tubule epithelium (2). The sulfur-containing thiol or further downstream electrophilic metabolites lead to tubular epithelial cell degeneration and necrosis.

feces (unpublished data) and other downstream metabolites of the β-lyase pathway, such as the S-glucuronide M1 and the thiomethyl M56 were observed at very low levels in urine and liver, respectively, in this study. Other potential contributing factors to sotorasib-related renal toxicity, which were not investigated here, include oxidative stress mediated by GSH depletion and accumulation of toxic metabolites following transporter inhibition in renal tubular epithelial cells (Ceckova et al., 2018; Tohyama et al., 2019).

Sotorasib-induced renal toxicity was observed in the rat, but not in the dog (up to 1000 mg/kg/day for 3 months). No signals of renal toxicity to date have been observed in sotorasib clinical trials (Hong et al., 2020; Li et al., 2021). Based on the weight of scientific evidence from nonclinical and clinical safety data, as well as published information on rat-specific renal tubular injury associated with the mercapturate pathway, the risk for sotorasib-related renal toxicity in the human is considered low.

There are several factors related to the mercapturate pathway that may play a role in the species-specific nature of the sotorasib-related renal toxicity. As discussed above, disposition of cysteine S-conjugate M10 in the rat renal tissue was considered to contribute to cysteine S-conjugate β-lyase mediated bioactivation. In a rat mass balance study with sotorasib, plasma C_{max} of M10 was 6590 ng eq./g (6590 ng/mL, assuming 1 g plasma $\approx$ 1 mL plasma) and was observed 0.5-h after a single oral dose of 60 mg/kg (unpublished data), which was a non-nephrotoxic dose in this study. At the highest dose tested in the clinic (960 mg), the human plasma C_{max} of M10 did not exceed 2610 ng/mL and was observed at 5.9 to 24 h postdose (unpublished data). Therefore, greater and more rapid formation of M10 may contribute to greater susceptibility to renal toxicity in the rat.

Another important factor contributing to the greater susceptibility of the rat to sotorasib-related renal toxicity is species differences in metabolic enzymes. Various phase I and II metabolizing enzymes involved in the course of renal toxicity onset are expressed in renal epithelium and the expression of these enzymes is species-dependent (Barnett and Cummings, 2018; Cooper and Hanigan, 2018). It has been reported that rat renal tissue is more susceptible than that of human to renal toxicity caused by β-lyase mediated bioactivation because of greater specific activities of cysteine S-conjugate β-lyases (Green et al., 1990; Lash et al., 1990; McCarthy et al., 1994; Iyer and Anders, 1996; Gul Altuntas and Kharasch, 2002; Anders, 2005) and allometric scaling (Anders, 2005). One relevant example of species-dependent metabolism leading to nephrotoxicity is efavirenz, a nonnucleoside reverse transcriptase inhibitor used in antiretroviral therapy. Rats are susceptible to nephrotoxicity, characterized by proximal tubular epithelial cell necrosis, while the cynomolgus monkey and humans are not (Gerson et al., 1999). In a comparison of metabolites produced by rats, monkeys, and humans, the difference in susceptibility was attributed to a unique glutathione adduct that is further metabolized by mercapturate pathway enzymes (Mutlib et al., 2000). Another relevant example illustrating the association between nephrotoxicity and species-dependent differences in mercapturate and β-lyase pathway enzyme activities is hexachlorobutadiene, for which the rates of key metabolic steps were several fold lower in humans compared to rats (Green et al., 2003).

In our mechanistic rat study, renal tubular degeneration and necrosis at 750 mg/kg was associated with an increase in clinical pathology biomarkers of renal function and renal injury including, including serum

UN and creatinine and urine KIM-1 and clusterin; therefore, toxicologically significant renal toxicity was monitorable using these biomarkers in the context of this study. Clinical trials with sotorasib have included monitoring of renal function with regular measurement of serum creatinine and/or estimated creatinine clearance along with microscopic examination of urine sediment. To date, there has been no signal identified in the clinical studies suggestive of renal toxicity (Hong et al., 2020; Li et al., 2021).

5. Conclusion

The kidney was identified as a target organ of toxicity in the sotorasib toxicology studies in the rat but not the dog. Sotorasib-related renal toxicity was characterized by tubular epithelial cell degeneration and necrosis, primarily restricted to the proximal tubules in the OSOM, a region rich in metabolizing enzymes. Mercapturate pathway metabolites were temporally and spatially associated with renal toxicity. The data presented here support the hypothesis that sotorasib-related renal toxicity in the rat is mediated by a nephrotoxic metabolite derived from the mercapturate/β-lyase pathway. The rat is reported to be particularly susceptible to the formation of nephrotoxic metabolites via this metabolic pathway. The greater understanding of the mechanism driving sotorasib-induced renal toxicity in the rat aids the overall translational risk assessment and leads to the conclusion that human risk is low. The low risk for humans is based on absence of renal toxicity in the dog or in the clinic to date, the greater and more rapid systemic formation of the cysteine conjugate M10 as a source metabolite of the subsequent putative nephrotoxic metabolite in the rat compared to human, and literature based reports of the higher susceptibility of the rat to nephrotoxic metabolites formed via the β-lyase pathway.

Funding

Declaration of Competing Interest

The authors declare that they have no known competing financial interests or personal relationships that could have appeared to influence the work reported in this paper.

Appendix A. Supplementary data

Supplementary data to this article can be found online at https://doi.org/10.1016/j.taap.2021.115578.

References

AACR, 2017. AACR Project GENIE Consortium. AACR Project GENIE: powering precision medicine through an international consortium. Cancer Discov. 7, 818–831.

Anders, M.W., 2005. Formation and toxicity of anesthetic degradation products. Annu. Rev. Pharmacol. Toxicol. 45, 147–176.

Baillie, T.A., 2020. Approaches to mitigate the risk of serious adverse reactions in covalent drug design. Expert Opin. Drug Discovery 1–13.

Barbacid, M., 1987. ras genes. Annu. Rev. Biochem. 56, 779–827.

Barnett, L.M.A., Cummings, B.S., 2018. Nephrotoxicity and renal pathophysiology: a contemporary perspective. Toxicol. Sci. 164, 379–390.

Canon, J., Rex, K., Saiki, A.Y., Mohr, C., Cooke, K., Bagal, D., Gaida, K., Holt, T., Knutson, C.G., Koppada, N., Lanman, B.A., Werner, J., Rapaport, A.S., San Miguel, T., Ortiz, R., Osgood, T., Sun, J.R., Zhu, X., McCarter, J.D., Volak, L.P., Houk, B.E., Fakih, M.G., O'Neil, B.H., Price, T.J., Falchook, G.S., Desai, J., Kuo, J., Govindan, R., Hong, D.S., Ouyang, W., Henary, H., Arvedson, T., Cee, V.J., Lipford, J.R., 2019. The clinical KRAS(G12C) inhibitor AMG 510 drives anti-tumour immunity. Nature 575, 217–223.

Ceckova, M., Reznicek, J., Deutsch, B., Fromm, M.F., Staud, F., 2018. Efavirenz reduces renal excretion of lamivudine in rats by inhibiting organic cation transporters (OCT, Oct) and multidrug and toxin extrusion proteins (MATE, Mate). PLoS One 13, e0202706.

Chang, E.H., Gonda, M.A., Ellis, R.W., Scolnick, E.M., Lowy, D.R., 1982. Human genome contains four genes homologous to transforming genes of Harvey and Kirsten murine sarcoma viruses. Proc. Natl. Acad. Sci. U. S. A. 79, 4848–4852.

Cooper, A.J.L., Hanigan, M.H., 2018. Metabolism of glutathione S-conjugates: multiple pathways. Comprehensive Toxicol. 363–406.

Gerson, R., Mutlib, A., Meunier, P., Haley, P., Gan, L., Chen, H., Davies, M., Gemzik, B., Christ, D., Krahn, D.J.T.S., 1999. Species-specific nephrotoxicity induced by glutathione conjugation of efavirenz in rats, 48, 1833.

Green, T., Odum, J., Nash, J.A., Foster, J.R., 1990. Perchloroethylene-induced rat kidney tumors: an investigation of the mechanisms involved and their relevance to humans. Toxicol. Appl. Pharmacol. 103, 77–89.

Green, T., Lee, R., Farrar, D., Hill, J., 2003. Assessing the health risks following environmental exposure to hexachlorobutadiene. Toxicol. Lett. 138, 63–73.

Gul Altuntas, T., Kharasch, E.D., 2002. Biotransformation of L-cysteine S-conjugates and N-acetyl-L-cysteine S-conjugates of the sevoflurane degradation product fluoromethyl-2,2-difluoro-1-(trifluoromethyl)vinyl ether (compound A) in human kidney in vitro: interindividual variability in N-acetylation, N-deacetylation, and beta-lyase-catalyzed metabolism. Drug Metab. Dispos. 30, 148–154.

Hamilton, R.A., Garnett, W.R., Kline, B.J., 1981. Determination of mean valproic acid serum level by assay of a single pooled sample. Clin. Pharmacol. Ther. 29, 408–413.

Hanna, P.E., Anders, M.W., 2019. The mercapturic acid pathway. Crit. Rev. Toxicol. 49, 819–929.

Hong, D.S., Fakih, M.G., Strickler, J.H., Desai, J., Durm, G.A., Shapiro, G.I., Falchook, G. S., Price, T.J., Sacher, A., Denlinger, C.S., Bang, Y.-J., Dy, G.K., Krauss, J.C., Kuboki, Y., Kuo, J.C., Coveler, A.L., Park, K., Kim, T.W., Barlesi, F., Munster, P.N., Ramalingam, S.S., Burns, T.F., Meric-Bernstam, F., Henary, H., Ngang, J., Ngarmchamnanrith, G., Kim, J., Houk, B.E., Canon, J., Lipford, J.R., Friberg, G., Lito, P., Govindan, R., Li, B.T., 2020. KRASG12C inhibition with sotorasib in advanced solid tumors. N. Engl. J. Med. 383 (13), 1207–1217.

Horvath, J.J., Witmer, C.M., Witz, G., 1992. Nephrotoxicity of the 1:1 acrolein-glutathione adduct in the rat. Toxicol. Appl. Pharmacol. 117, 200–207.

Iyer, R.A., Anders, M.W., 1996. Cysteine conjugate beta-lyase-dependent biotransformation of the cysteine S-conjugates of the sevoflurane degradation product compound A in human, nonhuman primate, and rat kidney cytosol and mitochondria. Anesthesiology 85, 1454–1461.

Karnoub, A.E., Weinberg, R.A., 2008. Ras oncogenes: split personalities. Nat. Rev. Mol. Cell Biol. 9, 517–531.

Kirsten, W.H., Mayer, L.A., 1967. Morphologic responses to a murine erythroblastosis virus. J. Natl. Cancer Inst. 39, 311–335.

Lanman, B.A., Allen, J.R., Allen, J.G., Amegadzie, A.K., Ashton, K.S., Booker, S.K., Chen, J.J., Chen, N., Frohn, M.J., Goodman, G., Kopecky, D.J., Liu, L., Lopez, P., Low, J.D., Ma, V., Minatti, A.E., Nguyen, T.T., Nishimura, N., Pickrell, A.J., Reed, A. B., Shin, Y., Siegmund, A.C., Tamayo, N.A., Tegley, C.M., Walton, M.C., Wang, H.L., Wurz, R.P., Xue, M., Yang, K.C., Achanta, P., Bartberger, M.D., Canon, J., Hollis, L.S., McCarter, J.D., Mohr, C., Rex, K., Saiki, A.Y., San Miguel, T., Volak, L.P., Wang, K.H., Whittington, D.A., Zech, S.G., Lipford, J.R., Cee, V.J., 2020. Discovery of a covalent inhibitor of KRAS(G12C) (AMG 510) for the treatment of solid tumors. J. Med. Chem. 63, 52–65.

Lash, L.H., Nelson, R.M., Van Dyke, R.A., Anders, M.W., 1990. Purification and characterization of human kidney cytosolic cysteine conjugate beta-lyase activity. Drug Metab. Dispos. 18, 50–54.

Li, B.T., Skoulidis, F., Falchook, G., Sacher, A., Velcheti, V., Dy, G.K., Price, T.J., Borghaei, H., Schuler, M., Kato, T., Takahashi, T., Spira, A., Ramalingam, S., Besse, B., Barlesi, F., Tran, Q., Ang, A., Anderson, A., Henary, H., Ngarmchamnanrith, G., Govindan, R., Wolf, J., 2021. PS02.07 - CodeBreak 100: Registrational Phase 2 Trial of Sotorasib in KRAS p.G12C Mutant NSCLC, 2020 World Conference on Lung Cancer, Singapore.

Lock, E.A., Antoine, D.J., 2018. 14.03 - renal xenobiotic metabolism. In: McQueen, C.A. (Ed.), Comprehensive Toxicology, Third edition. Elsevier, Oxford, pp. 30–55.

Maronpot, R.R., Yoshizawa, K., Nyska, A., Harada, T., Flake, G., Mueller, G., Singh, B., Ward, J.M., 2010. Hepatic enzyme induction: histopathology. Toxicol. Pathol. 38, 776–795.

McCarthy, R.I., Lock, E.A., Hawksworth, G.M., 1994. Cytosolic C-S lyase activity in human kidney samples-relevance for the nephrotoxicity of halogenated alkenes in man. Toxicol. Ind. Health 10, 103–112.

Miller, R.P., Tadagavadi, R.K., Ramesh, G., Reeves, W.B., 2010. Mechanisms of Cisplatin nephrotoxicity. Toxins (Basel) 2, 2490–2518.

Mutlib, A.E., Gerson, R.J., Meunier, P.C., Haley, P.J., Chen, H., Gan, L.S., Davies, M.H., Gemzik, B., Christ, D.D., Krahn, D.F., Markwalder, J.A., Seitz, S.P., Robertson, R.T., Miwa, G.T., 2000. The species-dependent metabolism of efavirenz produces a nephrotoxic glutathione conjugate in rats. Toxicol. Appl. Pharmacol. 169, 102–113.

NRC, 2011. Guide for the Care and Use of Laboratory Animals. National Academy Press, Washington, DC.

OLAW, 2015. Public Health Services Policy on Humane Care and Use of Laboratory Animals. National Institutes of Health: Office of Laboratory Animal Welfare.

Perazella, M.A., 2018. Pharmacology behind common drug Nephrotoxicities. Clin. J. Am. Soc. Nephrol. 13, 1897–1908.

Román, M., Baraibar, I., López, I., Nadal, E., Rolfo, C., Vicent, S., Gil-Bazo, I., 2018. KRAS oncogene in non-small cell lung cancer: clinical perspectives on the treatment of an old target. Mol. Cancer 17 (33), 14.

Rood, J.J.M., Jamalpoor, A., van Hoppe, S., van Haren, M.J., Wasmann, R.E., Janssen, M. J., Schinkel, A.H., Masereeuw, R., Beijnen, J.H., Sparidans, R.W., 2020. Extrahepatic metabolism of ibrutinib. Investig. New Drugs 39, 1–14.

Testa, B., Clement, B., 2015. Chapter 24 - biotransformation reactions and their enzymes. In: Wermuth, C.G., Aldous, D., Raboisson, P., Rognan, D. (Eds.), The Practice of Medicinal Chemistry, Fourth edition. Academic Press, San Diego, pp. 561–584.

Tohyama, K., Chisaki, I., Takai, Y., Handa, Y., Miyamoto, M., Amano, N., 2019. Relationship of MATE1 inhibition and cytotoxicity in nephrotoxicity: application for safety evaluation in early drug discovery. Toxicol. Sci. 170, 223–233.

Townsend, D.M., Hanigan, M.H., 2002. Inhibition of gamma-glutamyl transpeptidase or cysteine S-conjugate beta-lyase activity blocks the nephrotoxicity of cisplatin in mice. J. Pharmacol. Exp. Ther. 300, 142–148.

Tsuchida, S., 2002. Glutathione transferases. In: Bertino, J.R. (Ed.), Encyclopedia of Cancer, Second edition. Academic Press, New York, pp. 297–307.

Zhang, L., Hanigan, M.H., 2003. Role of cysteine S-conjugate beta-lyase in the metabolism of cisplatin. J. Pharmacol. Exp. Ther. 306, 988–994.